IEEE Access
Multidisciplinary | Rapid Review | Open Access Journal

Received October 1, 2018, accepted October 22, 2018, date of publication November 13, 2018,
date of current version December 7, 2018.

Digital Object Identifier 10.1109/ACCESS.2018.2878493

Power Quality Improvement and Low Voltage Ride Through Capability in Hybrid Wind-PV Farms Grid-Connected Using Dynamic Voltage Restorer

ABDELKRIM BENALI[1], MOUNIR KHIAT[1], TAYEB ALLAOUI[2], AND MOULOUD DENAÏ[3]
[1]SCAMRE Laboratory, Electrical Engineering Department, ENP, Oran 31000, Algeria
[2]Energetic Engineering and Computer Engineering Laboratory, Engineering Department, Ibn Khaldoun University, Tiaret 14000, Algeria
[3]School of Engineering and Technology, University of Hertfordshire, Hertfordshire AL10 9AB, U.K.

Corresponding author: Abdelkrim Benali (benaliabd@yahoo.fr)

ABSTRACT This paper proposes the application of a dynamic voltage restorer (DVR) to enhance the power quality and improve the low voltage ride through (LVRT) capability of a three-phase medium-voltage network connected to a hybrid distribution generation system. In this system, the photovoltaic (PV) plant and the wind turbine generator (WTG) are connected to the same point of common coupling (PCC) with a sensitive load. The WTG consists of a DFIG generator connected to the network via a step-up transformer. The PV system is connected to the PCC via a two-stage energy conversion (dc–dc converter and dc–ac inverter). This topology allows, first, the extraction of maximum power based on the incremental inductance technique. Second, it allows the connection of the PV system to the public grid through a step-up transformer. In addition, the DVR based on fuzzy logic controller is connected to the same PCC. Different fault condition scenarios are tested for improving the efficiency and the quality of the power supply and compliance with the requirements of the LVRT grid code. The results of the LVRT capability, voltage stability, active power, reactive power, injected current, and dc link voltage, speed of turbine, and power factor at the PCC are presented with and without the contribution of the DVR system.

INDEX TERMS Active power, DC-link voltage DFIG, dynamic voltage restorer, LVRT, power factor, photovoltaic, voltage stability, reactive power.

I. INTRODUCTION

Global demand for electric power is growing and expanding. It is interesting to note the sharp increase in energy consumption in China since 1973, by a factor of 8.4 in 42 years, while the world's consumption increased by a factor of 4 and the world's population doubled. But in 2017, more than one billion people still did not have access to electricity. The two major sectors consuming electricity are the residential-tertiary sector and industry, however, this consumption has a huge impact on the environment due to the emission of CO_2 and consequently the global warming and greenhouse effect has forced several countries to sign an agreement to strengthen international action to maintain the global rise in temperature during this century well below 2 degrees Celsius at the 2015 climate change conference in Paris.

In this context, the energy policy of most countries around the world tends towards the exploitation of renewable energies as clean, available and cheaper source of energy in order to reach high levels of integration close to twenty percent by 2020 [1].

However, this resource is characterized by factors limiting its use on a large scale, namely intermittency due to variations in the uncontrollable primary source of energy, and the uncertainty of weather forecasts leading to uncertainty about production [2]. This challenge is more pronounced for wind generation because wind speed forecasts are less reliable than those of the sun irradiance. Another factor limiting the integration of these energies is the geographical location of the renewable energy production sites, which is generally located in remote areas where both wind and surface conditions are favorable in the case of wind and solar energy while the

transmission systems are relatively weak which causes new challenges for the control of the voltage and the compensation of reactive power.

The stochastic nature of these renewable energy sources can have an impact on the dynamic behavior of the grid and its stability during sudden and significant variations in the power delivered by one or more units of high power [2].

Similarly, if a renewable energy power plant operating at full power is suddenly disconnected due to a fault in the internal grid of the installation, the grid should remain stable and the voltage and frequency of the grid must be maintained within their admissible ranges [1]–[3]. Another factor that negatively impacts the power quality comes from the presence of modern power electronics technology as the output interface of power plants. These devices not only produce harmonics in the system, but are also very sensitive to distorted voltage signals [4].

To overcome these constraints and ensure the stability of the electric power system connected to large amounts of variable energy resources, the operators of energy systems have resorted to explore multiple technical solutions.

The proposed solutions have two components; one is regulatory where the technical grid code, directives and conditions dedicated to the integration of renewable energy sources into the grid required by the grid operators and the other solutions are technical ones.

One of the most important grid code requirements is the Low Voltage Ride Through (LVRT) capability, which means that the renewable energy conversion system must remain connected during grid faults and supply reactive power to support the grid [5]. These requirements have been applied to wind turbines only so far, but recently photovoltaic generators are also required to fulfill these grid codes.

The prospects of power generation from hybrid energy systems are proving to be very promising and reliable [6]. Muyeen [7] proposed a static synchronous compensator (STATCOM) combined with a small series dynamic braking resistor (SDBR) to enhance the stability of a grid-connected wind farm composed of a fixed-speed wind turbine generator system (WTGS). A DFIG and flywheel energy storage system was studied in [8] and the proposed control scheme was designed to ensure that the grid power is isolated from wind power output fluctuations. Rashid and Ali [9] applied a nonlinear control based on a modified bridge type fault current limiter (NCMBFCL) to improve the LVRT performance of a DFIG based wind farm subjected to symmetrical and unsymmetrical faults. Dosoglu and Arsoy [10] and Dosoglu [11] analyzed a system consisting of a supercapacitor energy storage coupled to the DFIG for a grid integrated wind generator DFIG and studied the transient behavior and LVRT capability of the system with and without energy storage system (ESS).

To enhance the LVRT capability of a grid-integrated DFIG-based wind farm, a STATCOM and supercapacitor energy storage system have been proposed in [12]. In [13], a new stator damping resistor unit (SDRU) and rotor current control (RCC) for grid-connected DFIG-based wind turbine has been studied. Other devices commonly used in distribution networks to protect critical loads against voltage disturbances are known as D-FACTS and include: D-STATCOM (Static Dispensing Compensator), DVR (Dynamic Voltage Restorer) and UPQC (Unified Power Quality Conditioner).

The DVR has the ability to attenuate voltage disturbances. It is generally installed between the load and the source in the distribution system to provide rapid support of the voltage by injecting the required voltage in series with the mains voltage through an injection transformer [14].

This paper presents a simulation study to demonstrate the effectiveness of the DVR to mitigate voltage disturbances, minimize their impact on the overall stability of the transmission and distribution network, and improve the LVRT capability when the network is connected to a hybrid PV-wind system.

A DVR based on fuzzy logic control and phase compensation technique is designed and evaluated under various fault conditions such as short-circuits and voltage sags.

It is well known that active power recovery and no excessive reactive power absorption are essential for system security and sufficiently quick active power recovery is essential for frequency stability in the overall grid whereas large reactive power absorption could have a negative impact on voltage recovery or even drive the system into a local voltage collapse. This contribution is aimed to demonstrate that the DVR with the proposed control scheme is able to provide these features for the hybrid PV-Wind generators coupled to grid system.

The remaining of the paper is organized as follows: Section 2 describes the configuration of the hybrid distributed generation system which consists of photovoltaic and wind power plants and develops a detailed simulation model of the DC/DC and DC/AC converters. Section 3 describes the topology of the DVR and its basic scheme. Section 4 reiterates the need to introduce new grid codes related to the penetration of renewable energy power plants into the grid. Section 5 presents the simulation results, including the assessment of the LVRT capability under various disturbances. Finally, Section 6 concludes this work.

II. PROPOSED SIMULATED SCENAROS AND SYSTEM DESCRIPTION

The choice of photovoltaic energy or wind turbine or both depends on the availability of the renewable resource over time and also is abundance at the site of installation. Currently, solar and wind are the most commonly adopted and most easily exploitable renewable energy sources.

Several studies have shown that solar radiation and wind speed distributions often have complementary behavior, and consequently in many cases a hybrid configuration combining photovoltaic and wind generators is adopted [4].

Particularly, PV and wind energy technologies have enhanced their integration in hybrid power system configurations. This combination is considered as one of the

most efficient configurations which can be used either in grid-connected or standalone modes. Solar and wind energies are complementary in nature [4], [15], [16] and therefore can be utilized to overcome the problem of intermittency and provide a more reliable power with better quality to the electricity grid and remote areas [17], [18].

In recent years, several research studies have been carried out on PV-wind hybrid systems [17]. This study summarizes several research articles in the literature on PV-wind hybrid power system. Among these, a few studies proposed the integration of PV and DFIG-based wind power in a hybrid configuration to supply sustainable power to remote load centers. This configuration has several advantages including simple design, decoupling control of the active and reactive powers, partially rated converters, and maximum wind energy extraction form the turbine [17].

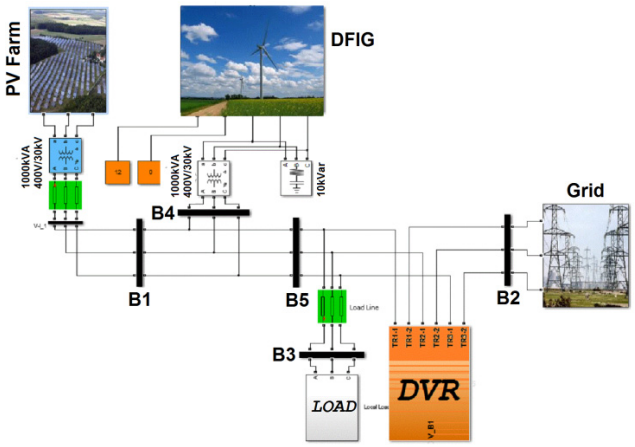

FIGURE 1. PV-WTG hybrid system with DVR and a load connected to grid.

The proposed topology is illustrated in Fig. 1. It consists of a 500 kW PV plant interconnected to a distribution system via a three phase PWM inverter with a three phase AC throttle filter and a step-up transformer.

The DFIG has a nominal output power of 500 kW and is connected to the grid at the PCC via a step-up transformer and supplying the load. Thus, the estimated total power delivered by the hybrid system is 1 MW.

This is a typical connection of a hybrid PV-WTG however there are other topologies of connections. The comparative study presented in [19] concludes that: (i) In terms of power efficiency, the single stage topology is better, (ii) For the DC link voltage stability and reduced total harmonic distortion in the AC side voltage, the two-stage topology is preferred, (iii) With regard to the maximum power tracking precision, within an acceptable error range of controller oscillation and power losses in the AC-side filter, both topologies can satisfy these requirements.

In [20], transformer-less inverters are employed to enhance the efficiency, reduce the size and lower the cost of the circuit. Because of their high efficiency, transformer-less PV systems, are becoming more popular than conventional PV systems, especially in European markets [20].

The simulation scenarios presented in this paper are carried out as follows:

1. The DVR is disconnected and no fault is applied.
2. The DVR is also disconnected but the fault is applied.
3. Same scenarios as above but with the DVR in operation.

The PV farm is subjected to the solar irradiance described in Fig. 3 and the WTG is running with a wind speed of 12 m/s during the simulation time of 5 seconds.

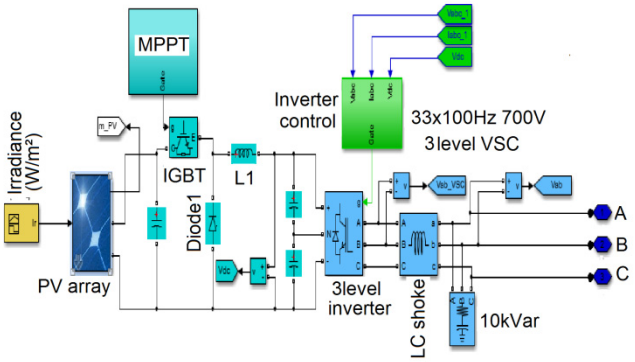

FIGURE 2. PV farm of 500 kW connected to grid via an inverter related to 500kVA-400V/30kV transformer.

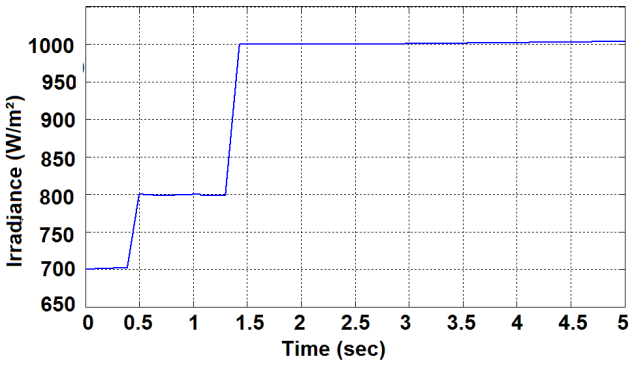

FIGURE 3. Solar irradiance at 25řC.

A. PHOTOVOLTAIC PLANT

The PV plant array consists of 16 series modules and 102 parallel strings (type: SunPower SPR-305-WHT).

The PV model used in the paper is based on the two-diode equivalent circuit shown in Fig. 4.

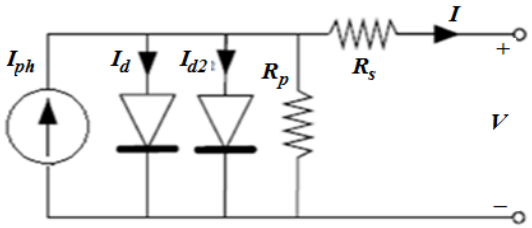

FIGURE 4. PV cell circuit model [21].

The PV cell total current in the equivalent circuit shown in Fig. 4 is expressed by [21]:

$$I = I_{ph} - I_{s1}\left(e^{q\frac{V+IR_s}{\eta kT}} - 1\right) - I_{s2}\left(e^{q\frac{V+IR_s}{\eta_2 kT}} - 1\right) - \frac{V+IR_s}{R_p} \quad (1)$$

Where η is the ideality factor.

Assuming that all the cells are identical and operating under the same operating conditions [21]:

$$R_{p,field} = \frac{N_s}{N_p}.R_{p,cell} \quad (2)$$

The photovoltaic power conversion control is based on maximum power point tracker (MPPT) which allows high efficiency power transfer and depends on both the solar irradiance and the electrical characteristics of the load [5].

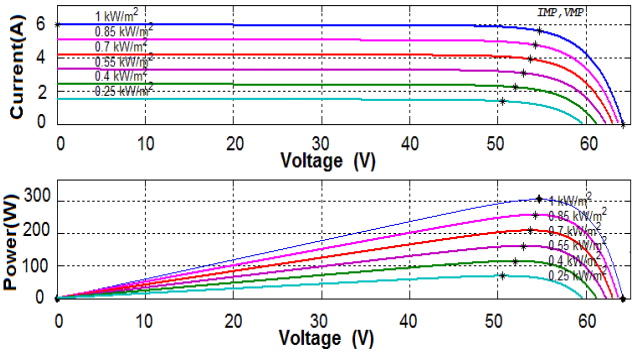

FIGURE 5. V–I and P-V characteristic of PV module under different solar irradiance and at 25řC with MPPT points in strings.

Fig. 5 shows the I-V and P-V characteristics of the PV module for different levels of solar irradiance.

As depicted in Fig. 5, the maximum power is defined by the largest rectangle area, $P_{MP} = V_{MP}I_{MP}$, obtainable from the I–V characteristic. The coordinates of the V_{MP} are found as:

$$\frac{dP}{dV}|_{V=V_{MP}} = \frac{d(IV)}{dV}|_{V=V_{MP}} = (I + \frac{dI}{dV})|_{V=V_{MP}} = 0 \quad (3)$$

Then I_{MP} is determined by evaluating Equation 1 at $V = V_{MP}$ [21].

The PV array model is scaled to include 12 series modules and 102 parallel strings in order to deliver 500 kW at an irradiance of 1000W/m^2 and a DC voltage of $V_{DC} = 896$ PV applied to the boost converter as shown in Fig. 6.

There are several MPPT control methods proposed in the literature, some of them are very much similar in terms of their operating principle [22].

A classification of the most popular MPPT algorithms is depicted in Fig. 7. Fractional methods and Hill-climbing are widely used in commercial PV systems. Hill-climbing algorithms are the most popular methods used in practice due to their ease of implementation and tracking performance [23].

Among these methods, the Incremental Conductance (INC) Algorithm is selected and used in the present work.

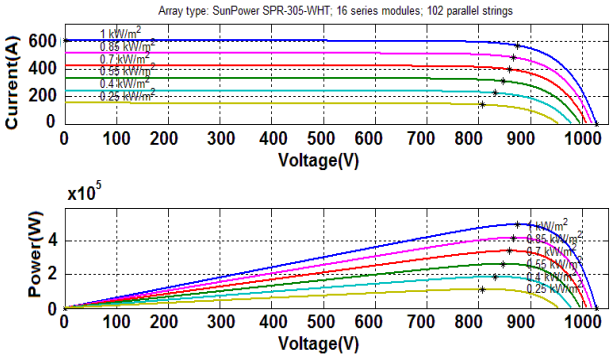

FIGURE 6. PV array power and current vs. array voltage.

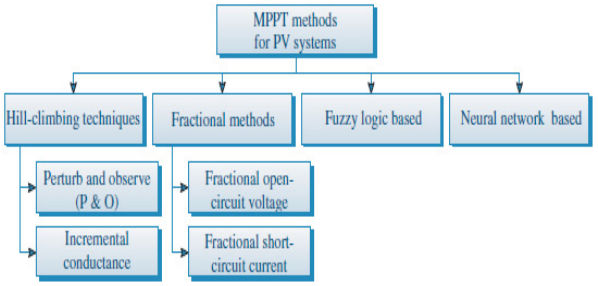

FIGURE 7. MPPT algorithm classification [23].

The INC approach can be regarded as an improved version of the Perturb and Observe (P&O) [21]. This method is quite similar to the P&O algorithm and is very effective for rapidly changing atmospheric conditions [23].

The slope of the power curve is obtained from

$$\frac{dP_{PV}}{dV_{PV}} = 0 \Rightarrow \frac{dI_{PV}}{dV_{PV}} = -\frac{I_{PV}}{V_{PV}} \quad (4)$$

$$\frac{dP_{PV}}{dV_{PV}} = \frac{d(I_{PV}V_{PV})}{dV_{PV}} = I_{PV} + V_{PV}\frac{dI_{PV}}{dV_{PV}} \quad (5)$$

Multiplying both sides of Equation (5) by I/V_{PV} gives:

$$\frac{1}{V_{PV}}\frac{dP_{PV}}{dV_{PV}} = \frac{I_{PV}}{V_{PV}} + \frac{dI_{PV}}{dV_{PV}} = G_{PV} + dG_{PV} \quad (6)$$

Where G and dGdenote the conductance and incremental conductance respectively.

A flowchart describing the INC algorithm is shown in Fig. 8. The algorithm can track the MPP and remains there until a change in dI_{PV} or dV_{PV} occurs due to a change in atmospheric conditions.

The behavior of G and dG is shown in Fig. 9.

Fig. 10 shows the circuit model of the DC-DC boost converter used in this work.

The critical values of the inductor and capacitances of the designed boost converter are: $L_1 = 30$ mH, $C = 100$ μF, $C_1 = C_2 = 120$ mF.

To ensure maximum power extraction from the PV source, the converter interfacing the PV system to the grid must be capable of self-adjusting its own parameters in real-time.

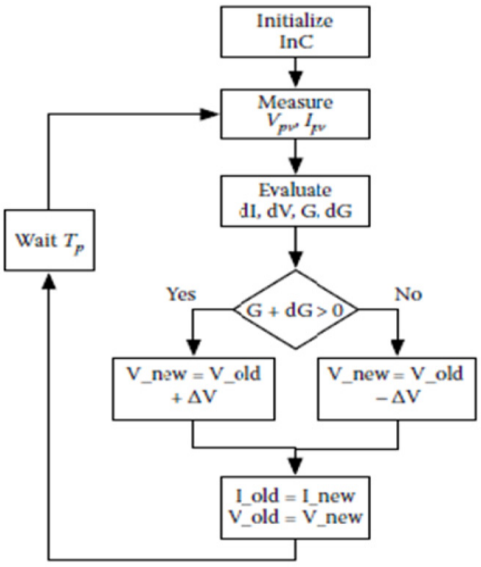

FIGURE 8. Flowchart of the incremental conductance algorithm [21].

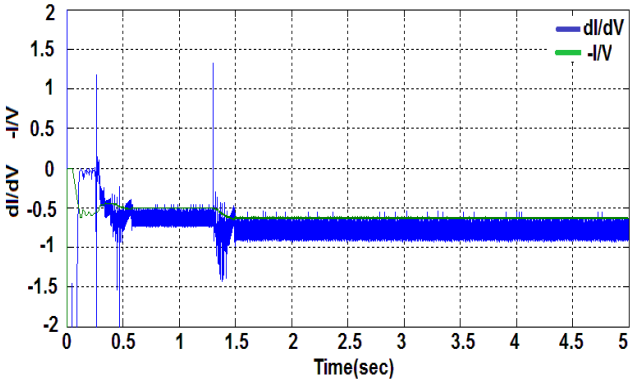

FIGURE 9. G_{PV} and dG_{PV} behavior during model simulation.

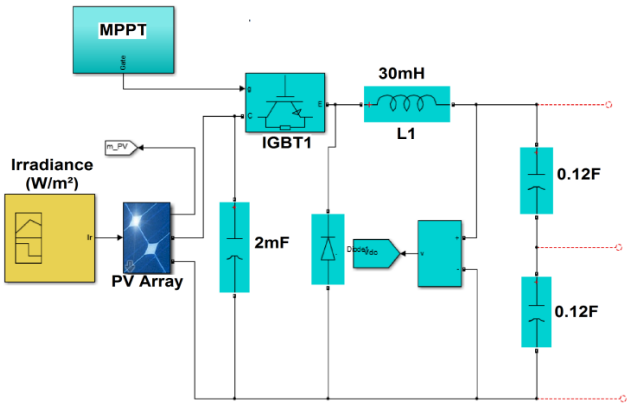

FIGURE 10. Boost converter circuit.

The most important application of these converters is the connection of renewable energy sources such as wind generators, photovoltaic modules, etc., to the electric network [24].

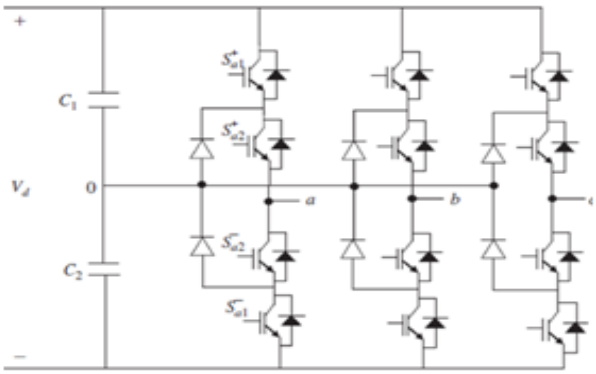

FIGURE 11. Three level inverter topology [25].

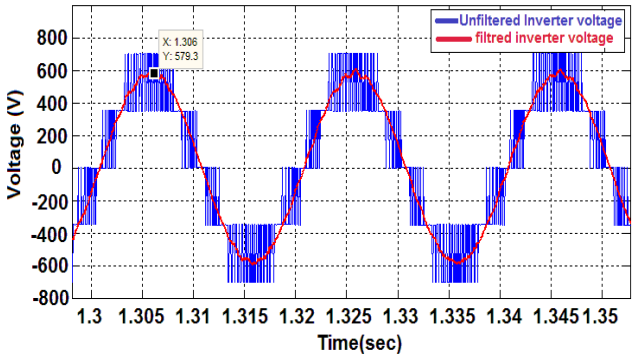

FIGURE 12. Output three-level inverter unfiltered and filtered voltage waveforms.

The three-level voltage source inverter topology shown in Fig. 11 is simulated in this work.

The V_{dc} boost converter reference output voltage is set at 714 V and the IGBT 3-level inverter uses PWM technique, (3.3 kHz carrier frequency) converting DC power from 714 Vdc source to 400 Vac, 50 Hz.

The grid is connected to the inverter via an inductive grid filter and a low frequency transformer to step-up the voltage from 0.4 kV to 3 0kV in order to reduce losses when PV energy is transmitted to the grid [23] and to filter out harmonic frequencies.

The 12 pulses required by the inverter are generated by the discrete three phase PWM generator.

For linear modulation ($m_a \leq 1$), the amplitude of the first harmonics is proportional to the modulation factor, so the expression of the phase voltage is given by [26]:

$$V_{1,LN} = m_a \frac{V_{DC}}{2} \tag{7}$$

B. MODELING OF THE WIND POWER PLANT

1) AERODYNAMIC MODELING OF THE WIND TURBINE

The kinetic energy from the wind is captured by the wind turbine and converted to mechanical power P_m [9], [23].The wind power plant consists of a single DFIG-based wind turbine producing 500 kW with 400 V_{ac} output voltage.

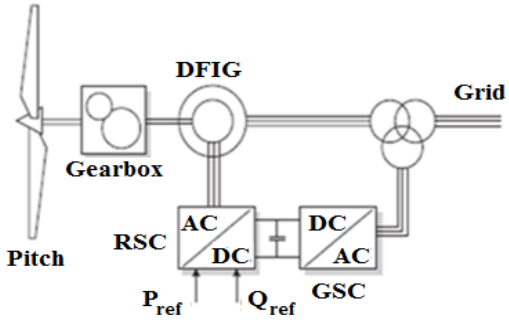

FIGURE 13. Doubly fed induction generator [3].

The power or torque of a wind turbine may be determined by several means [27].

The power P_m captured by the wind turbine is a function of the blade radius, the pitch angle, and the rotor speed [28]:

$$P_m = \frac{1}{2}\pi\rho C_p(\lambda, \beta)R^2\vartheta^3 \tag{8}$$

$$C_p(\lambda, \beta) = 0,22\left(\frac{116}{\lambda_i} - 0,4\beta - 5\right)e^{-\frac{21}{\lambda_i}} \tag{9}$$

$$\frac{1}{\lambda_i} = \frac{1}{\lambda + 0,08\beta} - \frac{0,035}{\beta^2 + 1} \tag{10}$$

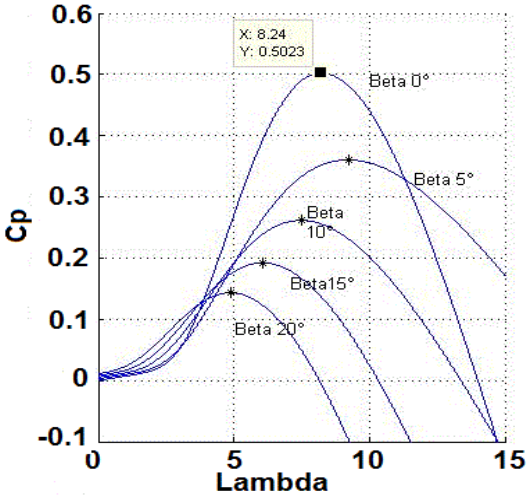

FIGURE 14. Power coefficient as a function of (λ_i) the speed ratio and the (β) the pitch angle.

Fig. 14 shows the simulated power curves for different wind speeds.

The mechanical equation of the system is given by [29]:

$$J_T\frac{d\Omega_{mec}}{dt} = C_{mec} - C_{em} - f\Omega_{mec} \tag{11}$$

Where J_T (kg.m^2) represents the total inertia of the generator, turbine, two shafts and gearbox, Ω_{mec} (rad/s) is the mechanical speed of the generator, C_{em} (N.m) is the electromagnetic torque produced by the induction generator, C_{mec} (N.m) is the torque produced by the wind turbine when referred to the shaft of the induction machine, and f (N.m.s.rad^{-1}) is the coefficient of viscous friction [23], [29].

2) DOUBLE FED INDUCTION GENERATOR (DFIG) MODELING

AC generators for renewable generation are classified into fixed and variable speed applications.

Fixed-speed generators are connected directly to the grid such as the synchronous generator (Permanent Magnet Synchronous Generator (PMSG)) and induction generator (Squirrel-cage Induction Generator). Variable-speed generators include induction generator with variable rotor resistance (Wound Rotor Induction Generator), Doubly Fed Induction Generator (DFIG) and Generator with Fully Rated Converter (FRC) [29].

One of the major disadvantages of fixed-speed generators besides their fixed speed range is the need for power factor correction at the terminals of the induction generator.

The main features of a wind turbine with fixed speed induction generator are:

- The squirrel cage induction generator is directly connected to the grid (robust and low-cost).
- The speed of the generator cannot be controlled (driven by the grid frequency).
- Wind fluctuations translate to active power fluctuation.
- Typical speed range ~2% of the rated speed.
- Gearbox necessary.

DFIGs have several attractive features such as small size and light weight, high output power and efficiency, low cost and variable-speed operation. Wind turbine based on DFIG have a share of approximately 50 % in the wind energy market and the active and reactive powers can be controlled independently due to d-q vector control of the converter [9], [16].

DFIGs have been reported to suffer reliability problems due to their brushes, slip-rings, and gearbox. They require regular maintenance due to brush wearing and the building-up of carbon on the internal components, which brings extra costs [30]. One of the main drawbacks of using DFIGs is their vulnerability to grid-side short circuits and voltage sags [31]

The DFIG consists of a wound rotor induction generator, two bi-directional voltage source converters with a back-to-back DC link, protection circuits, a gearbox and a turbine as shown in Fig. 13.

The stator of the machine is connected directly to the grid at system frequency while the rotor is fed from a power converter at slip frequency as seen in Fig. 13. The voltage at the stator and rotor terminals can vary depending on the size of the turbine and generator [9], [23].

The space-vector model of the DFIG can be represented in a synchronously rotating frame [23], [31]. The voltage equations for the dynamic model written in d-q Park model are given by:

$$V_{ds} = R_sI_{ds} + \frac{d\psi_{ds}}{dt} - \omega_s\psi_{qs} \tag{12}$$

$$V_{qs} = R_s I_{qs} + \frac{d\psi_{qs}}{dt} + \omega_s \psi_{ds} \quad (13)$$

The rotor equations:

$$V_{dr} = R_r I_{dr} + \frac{d\psi_{dr}}{dt} - \omega_r \psi_{qr} \quad (14)$$

$$V_{qr} = R_r I_{qr} + \frac{d\psi_{qr}}{dt} + \omega_r \psi_{dr} \quad (15)$$

The stator flux linkage equations are given by:

$$\psi_{ds} = L_s I_{ds} + L_m I_{dr} \quad (16)$$

$$\psi_{qs} = L_s I_{qs} + L_m I_{qr} \quad (17)$$

And the rotor flux linkages are:

$$\psi_{dr} = L_r I_{dr} + L_m I_{dr} \quad (18)$$

$$\psi_{qr} = L_r I_{qr} + L_m I_{qr} \quad (19)$$

The stator active and reactive powers are expressed by [32]:

$$P_s = \frac{3}{2}\left(V_{ds} I_{ds} + V_{qs} I_{qs}\right) \quad (20)$$

$$Q_s = \frac{3}{2}\left(V_{qs} I_{ds} - V_{ds} I_{qs}\right) \quad (21)$$

Where V, I, ψ, are the voltage, current and flux respectively. R and L denote the resistance and inductance respectively.

The Rotor Side Converter (RSC) controller regulates the injected active and reactive power into the PCC. The q-axis current component controls the active power based on the reference provided by the MPPT strategy. The d-axis controls the exchange of reactive power with the power system [28]. A detailed block diagram of the RSC control scheme is depicted in Figure 15.

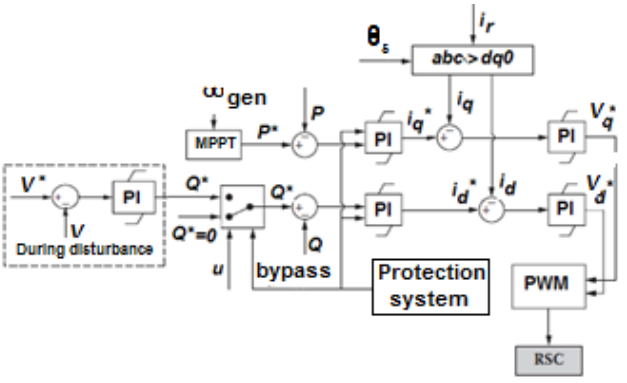

FIGURE 15. Power Control diagram of the rotor side converter [28].

The Grid Side Converter (GSC) controller aims to keep the DC-link voltage at its desired reference value despite any variations in the rotor power flow and the reactive power exchange with the grid [9], [23], [28]. With reference to Fig. 15, the DC-link voltage is compared with its reference value and the error is passed through a PI controller which generates the reference signal for the d-axis current.

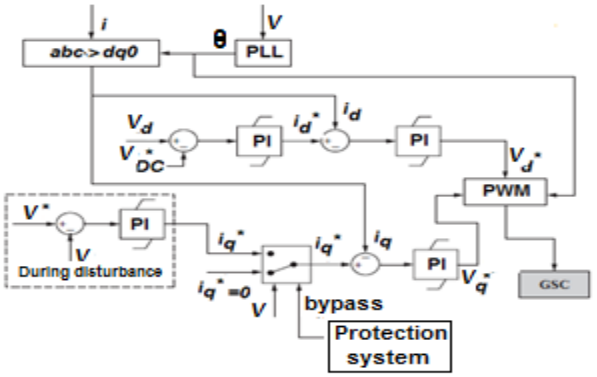

FIGURE 16. Power Control diagram of the grid side converter [28].

Referring to Fig. 16, the PI controller is used to control the d-axis current whose reference value is set to zero in order to ensure a unity power factor on the grid-side. The two cascaded control loops are used to regulate the DC bus voltage. The inner loop controls the q-axis current whereas the outer loop regulates the DC bus voltage. Then the reference voltages outputs of the PI controllers are transformed into abc using dq to abc transformation based on the stator angle obtained from the PLL control loop. The three-phase abc voltages are then compared with a carrier signals to generate the PWM signals to control the GSC switches.

III. DVR TOPOLOGY

Flexible AC Transmission System (FACTS) are power electronics-based devices which have the ability to control one or more parameters to enhance the capacity and improve the stability of the transmission system. Depending on the desired compensation, FACTS devices can be connected in series, parallel, or a combination of these configurations as shown in Fig. 17.

FACTS technologies offer new opportunities to control power flow and enhance the capacity of existing, as well as new and upgraded transmission lines [33]. These opportunities arise through the flexibility of FACTS devices and their ability to provide fast control of the electric parameters such as voltage, current, phase angle, and line impedances [33].

The first dynamic voltage restorer (DVR) was installed in South Carolina in August 1996 in 12.47 kV substations and was rated at 2 MVA to protect a load of 4 MVA [34].

The DVR consists of a VSC and its switching control, an energy storage device and a coupling transformer which in this case, is connected in series with the AC system, as shown in Fig. 18. This controller is suited for solving various problems related to power quality and reliability including [35]:

- Voltage disturbances such as sags and swells
- Voltage unbalances
- Voltage harmonics
- Power factor correction
- Outages.

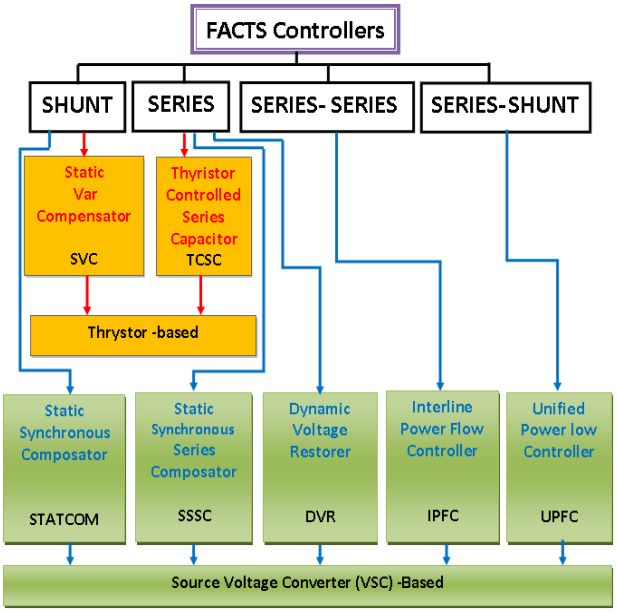

FIGURE 17. Basic types of FACTS controllers.

The DVR injects a three-phase AC voltage in series and synchronized with the distribution feeder voltage of the AC system. The injected voltage amplitude and phase can be varied to control the bi-directional exchange of active and reactive power between the DVR and AC system [28], [35].

The main role of the DVR is to balance and regulate the voltages and prevent harmonics from the source voltage to reach the load [35].

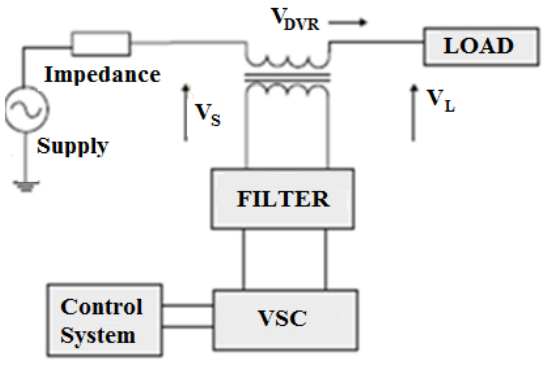

FIGURE 18. Basic schematic representation of the DVR [35].

The basic structure of the DVR shown in Fig. 18 consists of:

(1) Injection transformer
(2) Harmonic filter
(3) Energy storage device
(4) VSC
(5) DC charging circuit
(6) Control system.

The series voltage injected by the DVR can be written as follows:

$$V_{DVR} = V_L + Z_{TH} I_L - V_{TH} \tag{22}$$

Where V_L is the load voltage, Z_{TH} denotes the load impedance, I_L represents the load current and V_{TH} is the system voltage during fault.

The load current I_L is given by:

$$I_L = \frac{P_L + jQ_L}{V} \tag{23}$$

Taking V_L as a reference then the equation can be rewritten as:

$$V^*_{DVR} = V_L^{\angle 0} + Z_{TH}^{\angle(\beta-\theta)} - V_{TH}^{\angle\delta} \tag{24}$$

With

$$\theta = \tan^{-1}(\frac{\theta_L}{P_L}) \tag{25}$$

The complex power output of the DVR can be written as:

$$S_{DVR} = V_{DVR} I^*_{DVR} \tag{26}$$

A. FUZZY LOGIC CONTROLLER

Power systems are inherently nonlinear and the integration of renewable energy sources tends to make them more nonlinear due to the extensive use of power electronics switching devices. Therefore, nonlinear controllers such fuzzy logic controllers (FLC) are more suited for power systems control applications [9].

In Fig. 19 is shown the proposed FLC for the DVR

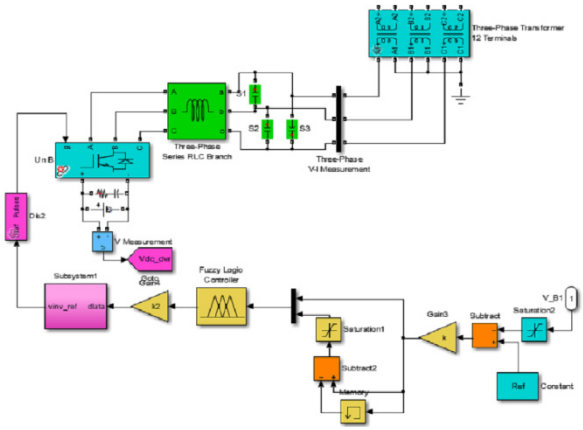

FIGURE 19. Designed DVR basic control scheme.

Fuzzy logic controllers have several advantages over conventional controllers. They are easy to design and implement and are able to handle a wider range of operating conditions. Self-organizing fuzzy controllers have the ability to automatically refine the membership functions [36].

Conventional control techniques based on linear system theory require a linearized model of the system and cannot guarantee a good performance over a wide operating range.

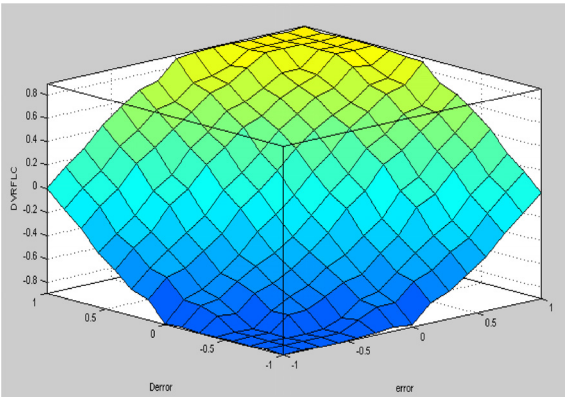

FIGURE 20. Designed DVR surface viewer of the fuzzy control rule.

In addition, model-based linear and nonlinear control solutions developed in the last three decades require precise mathematical models of the systems. However, most of those systems are complex and difficult to describe accurately using conventional mathematical relations; hence, these model-based design approaches may not provide satisfactory solutions. In contrast, FLC does not require a mathematical model of the system and has been successfully applied to various real-world systems characterized by uncertain environments and high nonlinearities [36].

Many studies have presented the DVR based on FLC and other studies have compared FLC controller and conventional PI controller. In [37], a DVR based on fuzzy polar controller is proposed to compensate for balanced voltage sags in distribution networks. The value of the injection voltage to compensate for the voltage drop caused by three phase fault is determined from the fuzzy polar controller parameters. The results have shown that the DVR based on the proposed fuzzy polar controller provides a better compensation of the balanced voltage sag than a conventional PI controller.

In [38], a DVR based on FLC is proposed to address power quality problems and the results are very significant for voltages of sensitive loads like adjustable speed AC drives.

Two control techniques, mainly PI control and FLC were investigated in [39] and [40]. The results for both controllers have demonstrated excellent performance and generated low total harmonic distortion (THD) ($< 5\%$). However, the FLC gave a better performance with a THD of only 0.64% as compared to 1.68% for PI.

B. ENERGY STORAGE SYSTEM(ESS)

During deep voltage sags, the ESS is rated to supply active power to the load. Various sources of storage can be used such as Lead-acid batteries, flywheel or Superconducting Magnetic Energy Storage (SMES). Alternatively, the required power on the DC side of the VSC could be provided by an auxiliary bridge converter that is fed from an auxiliary AC supply, SMES, supercapacitors and photovoltaic power source [16], [41].

The ESS of a DVR is often composed of a battery which provides the active power necessary to protect against longer interruptions.

Energy storage devices can be divided into three different categories depending on the required power capability: Small devices (<10 MW), medium devices (10 – 100 MW) and large devices (100 MW).

Batteries are included in the small and medium ESS categories since their wide range of capacities can vary from a few watts to a few megawatts. For a DVR system, the energy storage capacity must be large enough to meet the requirements for power quality and custom devices for a few seconds and a few cycles, respectively. According to Table 2 the DVR's DC link capacitor must have a storage capacity of 0.11 – 11 MJ with a discharging time period of a few seconds [41].

TABLE 1. Energy storage applications [41].

Storage Applications	Capacity of Storage	Period of Discharge
Grid level energy	11 MJ – 201 GJ	Few Seconds.–Few Days
Power Quality	0.11 – 11 MJ	Few Seconds
Custom Devices	0.11 – 11 MJ	Few Cycles

For modeling the DC link capacitor of the proposed DVR, the stored energy in a capacitor (J) is written as a function of the capacitance (F) and voltage (V) as follows [41]:

$$E = 0.5CV^2 \tag{27}$$

IV. GRID CODE

A. CODE REQUIREMENT

The major concerns for the interconnection of small scale renewable energy generation at the main power quality aspects that should be covered by connection conditions for renewable generation are power quality, voltage and reactive power control, power factor requirements and frequency requirements [42]. Grid operators have introduced new requirements for distributed power generations in a special way based on the above issues related to the ability to maintain the security and reliability of the power system while meeting the contractual power flow of the customers [43]. In [44] and [45] is presented a comprehensive and detailed comparative analysis between all members of the European integrated network. This study has focused on five selected European countries (Germany, France, UK, Poland and Turkey). New supplementary requirements of the future European grid codes by ENTSO-E and CENELEC are included in a consecutive analysis in order to identify necessary changes in the existing standards, which partially affect fundamental modifications for manufacturers.

A total of five major categories (active power control, reactive power supply, power quality (system disturbances), fault-behavior and protection concepts) are integrated in most of the European grid codes, differences can be found in the quantitative and qualitative design.

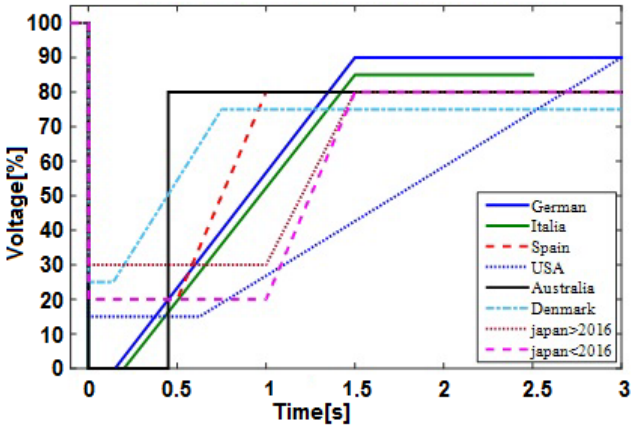

FIGURE 21. LVRT capability curves for different countries [20].

B. LVRT CAPABILITY

Most interconnection standards today require renewable energy farms to have the ability to handle severe disturbances, commonly referred to as fault ride through (FRT) capability or, in some cases, LVRT generally means that a generator is not allowed to disconnect in the case of a short-term voltage dip resulting from a short-circuit in the grid [1], [14]. LVRT capability probably represents the most important technical requirement and the most significant innovation for wind turbine generators and PV inverters with regard to system security [30], [44].

A comparative analysis of European Grid Codes and compliance standards for distributed power generation study is carried out in [28].

So the LVRT and HVRT capability are essential for secure operation of a power system with considerable shares of wind and PV generation. Without LVRT capability there would be a high risk that large amounts of wind and PV generation would disconnect if a single fault on a major transmission line were to cause a voltage dip over a wide area. The lost generation would have to be backed up by primary, secondary and tertiary control reserves and the associated costs would be massive.

LVRT capabilities for seven countries are illustrated in Fig. 21.

Therefore it is generally accepted nowadays that LVRT (and HVRT) capability is essential so as not to endanger the security of a power system.

V. ANALYSIS AND SIMULATION RESULTS

In order to evaluate the impact of the contribution of D-FACTS to wind farms linked to the grid, the DVR has been chosen as a case study. The designed DVR has the power of 4 MVA to regulate the voltage on a 30 kV distribution network connected to bus B2. A feeder transmits energy to a local load connected to the buses B5 which represents a plant absorbing continuously changing currents, thus producing a flicker of voltage.

The DVR adjusts the voltage at buses B2 and B5 by injecting an appropriate voltage. This voltage transfer is produced by the leakage reactor of the coupling transformer by generating a secondary voltage in phase with the primary voltage (gate side).

During normal operation, the DVR is in standby mode. When the fault occurs, the control circuit detects the disturbance in the supply voltage as seen in Fig. 25, and then the DVR injects the required voltage as shown in Fig. 26.

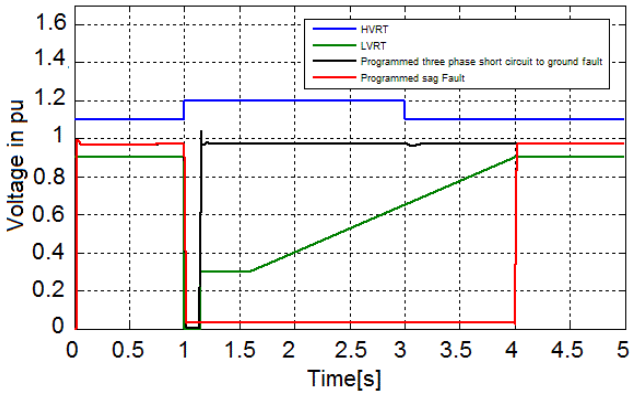

FIGURE 22. Voltage phase magnitude at PCC during faults with typical LVRT and HVRT characteristics requirements of Distributed Generation Code of Germany as an example.

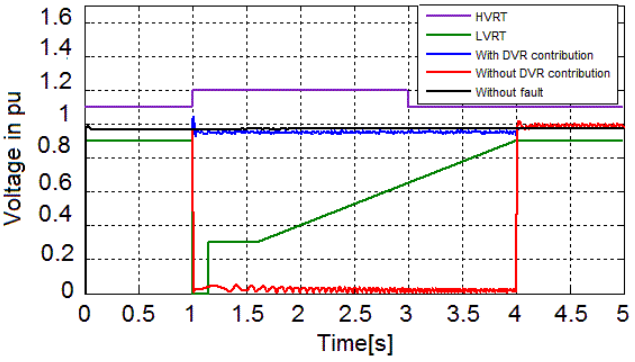

FIGURE 23. Voltage phase magnitude at PCC during sag fault.

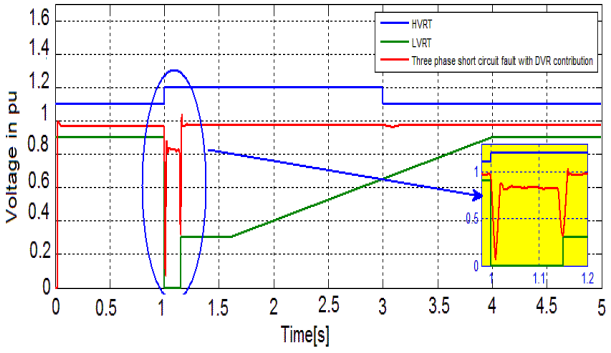

FIGURE 24. Voltage phase magnitude at PCC during short circuit fault.

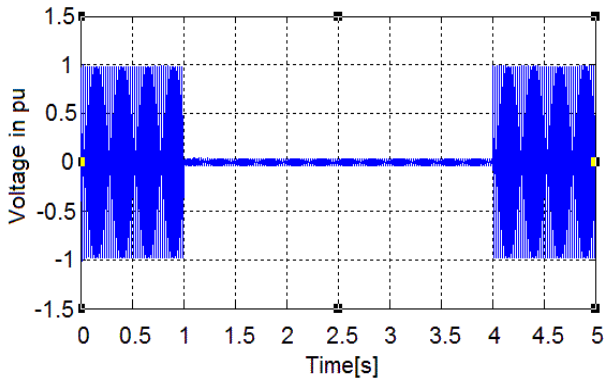

FIGURE 25. Phase voltage at PCC during sag fault.

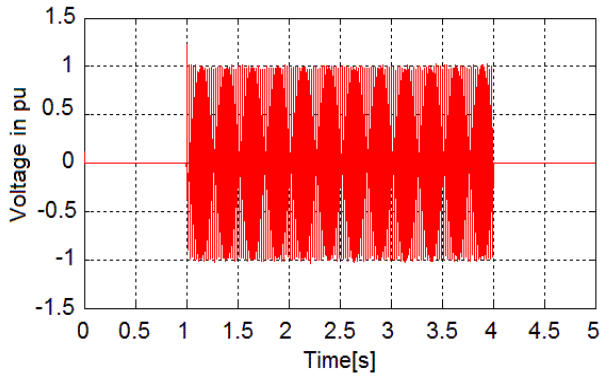

FIGURE 26. DVR voltage contribution at PCC during sag fault.

In the case of a voltage sag disturbance occurring at time t = 1s the system reaches the steady state after 2 cycles of oscillations which correspond approximately 0.026 s as shown in Fig. 23.

When the short circuit voltage occurs at t = 1s and after a transient of about 0.026 s duration, the steady state is reached, and a DVR voltage is injected as seen in Fig. 27.

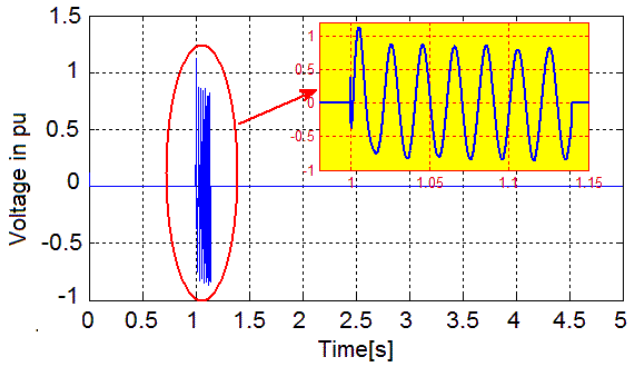

FIGURE 27. Phase voltage at PCC during short circuit fault.

Fig. 28 shows the total active power generated by both the WTG and the PV farm at the PCC. Overshoots and oscillations can be observed in the active power for 2 cycles

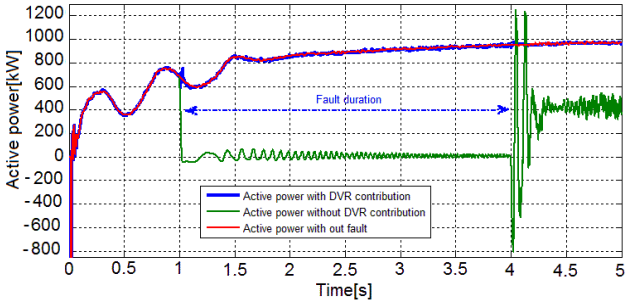

FIGURE 28. Total active power of hybrid system at PCC injected to grid.

of transient and then are completely damped by the DVR. Without DVR, during fault the active power has collapsed to zero until the end of fault where large oscillations appeared and lasted for 15 cycles. The response was then stabilized after 400 kW of active power generated by the PV farm was injected while wind generation has stopped as shown in the Fig. 27 and Fig. 29. The active powers generated by PV farm and WTG are shown in Fig. 29 and Fig. 30 respectively.

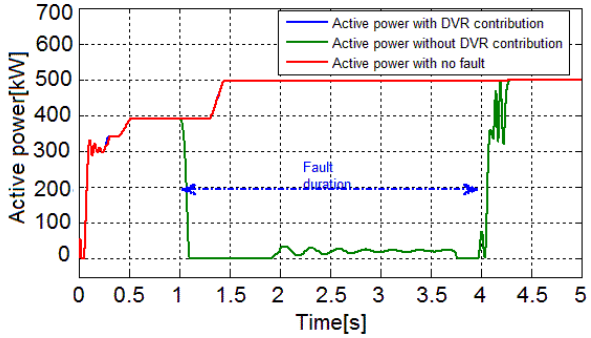

FIGURE 29. PV active power at PCC injected to grid.

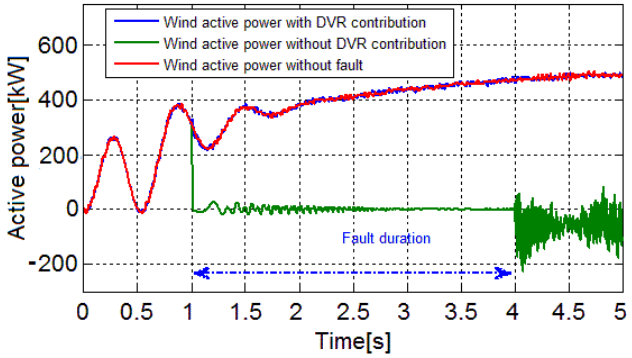

FIGURE 30. Wind active power at PCC injected to grid.

Fig. 33 shows the reactive power flow at the PCC. At the end of the sag fault, the oscillations of reactive power are larger in magnitude, in direction and duration when the DVR is not applied as compared to the case with DVR. After a

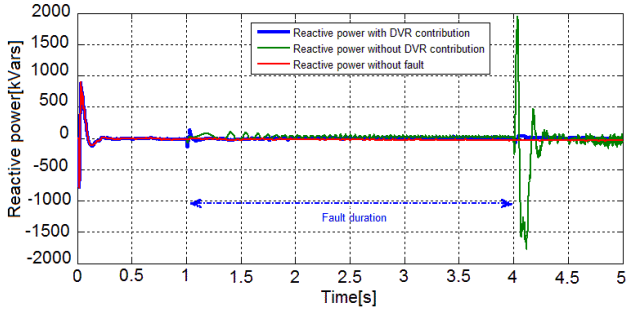

FIGURE 31. Total reactive power of hybrid system at PCC injected to grid.

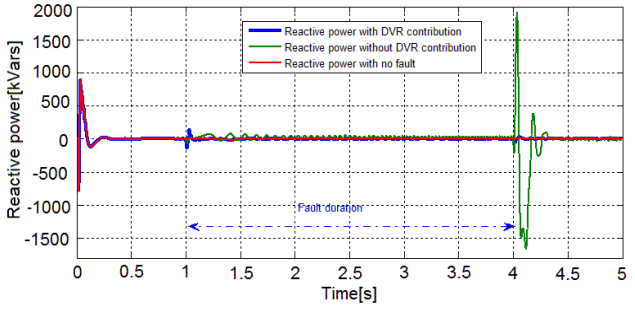

FIGURE 32. PV reactive power at PCC injected to grid.

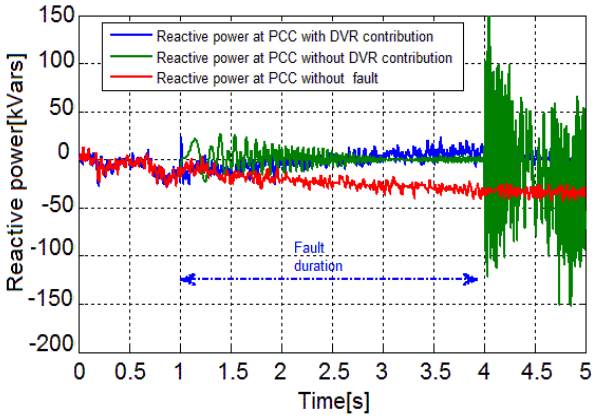

FIGURE 33. Wind reactive power at PCC injected to grid.

short oscillation at the beginning of the fault, a large overshoot appears at t = 4 s when +2 MVars are injected and suddenly the reactive power has decreased to −1.75 MVars at t = 4.12 s, then after several oscillations it has been stabilized very far to the end of the sag fault at t = 4.3 s as compared with the case with DVR where the oscillations have been completely damped at t = 4.13 s.

The individual reactive powers generated by the PV farm and WTG are plotted in Fig. 31 and Fig. 32 respectively.

The produced reactive power at the PCC is maintained at zero by both PV farm and WTG in order to keep the PF at unity as possible.

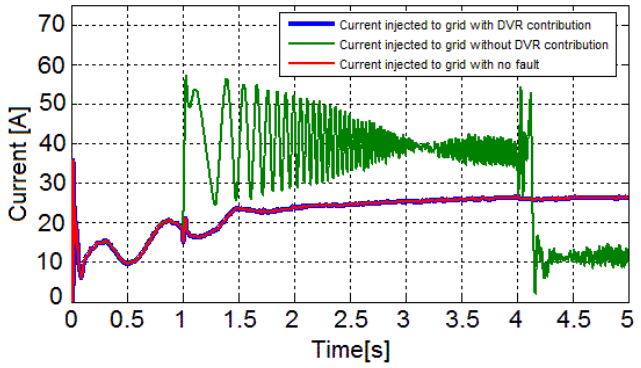

FIGURE 34. Total PV-WT current injected to grid at PCC.

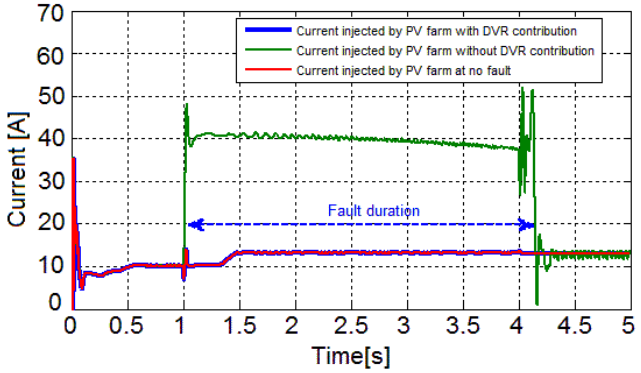

FIGURE 35. PV current injected at PCC.

Fig. 36 shows the total current injected from the PV farm and WTG into the grid at PCC. It is seen that during the voltage sag fault the current has increased from the normal consumed current of 19.07 A to the fault consumed reactive current of 57 A in the case without DVR and a severe current oscillations around 40 A are produced. Also it can be seen that the current has increased despite the voltage has decreased (sag voltage); this is the contribution of the PV system inverter in order to regulate its voltage at bus B1.

Similarly, it can be noted that the same contribution of the PV system inverter at the voltage sag fault when the current has increased from normal consumed current of 10.07 A to fault consumed current of 40 A and suddenly collapse to 10 A at the end of the sag fault and finally stabilizes after several overshoots as shown in Fig. 35.

The contribution of the DVR in stabilizing the current at the normal consumed value is reached rapidly and smoothly. The contribution of the DVR in maintaining the injected current at normal values during faults is clearly demonstrated.

Also as shown in Fig. 36, in the case of a sag fault and without DVR contribution, the WTG went out of service after approximately 3 s and the PV farm continues to generate power alone.

Fig. 37 shows the behavior of the PCC power factor. Under normal operation of the system, the PF is kept to unity by introducing 10 kVars capacitor in bus B1 and WTG at bus

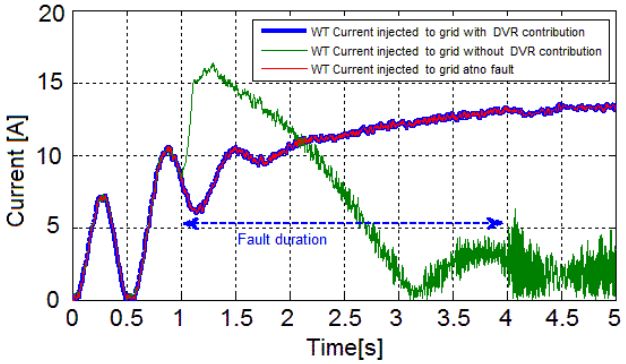

FIGURE 36. WT current injected at PCC to grid.

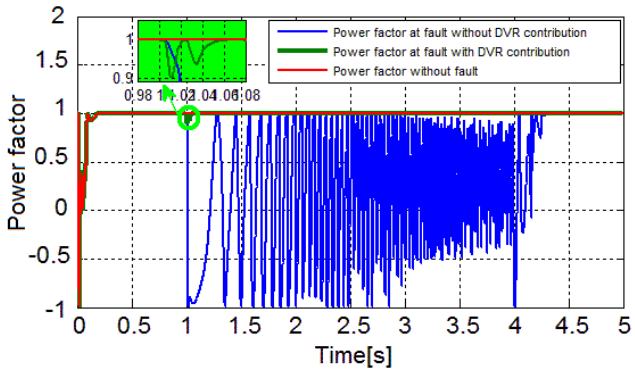

FIGURE 37. Power factor at PCC.

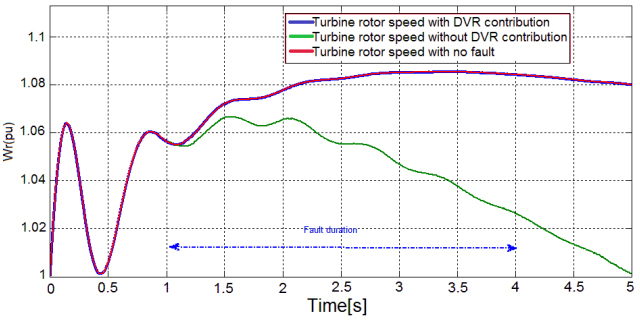

FIGURE 38. Turbine rotor speed.

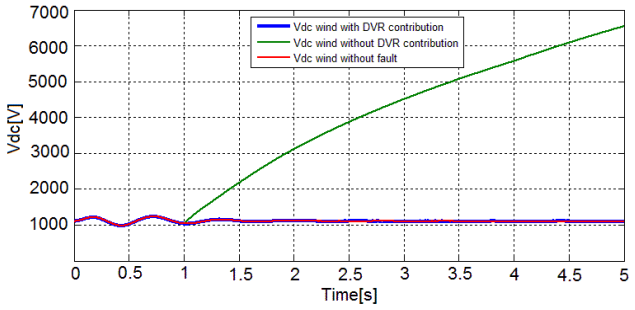

FIGURE 39. V_{dc} link at WTG inverter.

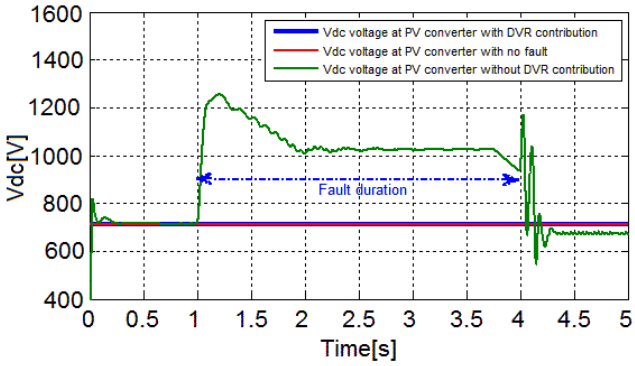

FIGURE 40. V_{dc} link voltage at PV inverter.

TABLE 2. System parameters.

Parameters		Value
MV grid	Nominal grid L-L voltage	30kV
	Frequency	50Hz
DVR	Inverter filter inductance	1,2mH
	Inverter filter capacitance	970µF
	Dc link capacitance	10mF
DFIG	Nominal power	500kw
	frequency	50Hz
	Nominal L-L	400V
Photovoltaic	Plant capacity	500kW
	V_{DC}	896V
	Parallel Strings	102
	Series modules	12
Step-up Transformer	Nominal power	1MVA
	Primary voltage	0,4kV
	Secondary voltage	30kV

B4 as shown Fig.1 in order to completely transfer the active power produced by the photovoltaic and WTG farms to the grid and to the load.

As shown in Fig. 37, in the event of a sag voltage fault and with the DVR contribution, the system is operating within acceptable limits $PF_{min} = 0.9$ as indicated at the beginning of the disturbance (1 s). However without the DVR, the PF dropped considerably and excessive oscillations appeared during the fault time.

It can be concluded that the PF at the PCC is well corrected by the contribution of the DVR during a voltage fault.

With regard to the impact of sag voltage disturbance on the mechanical parts of the WTG, it can be observed from Fig. 38 that the sag fault of the power grid can lead to oscillation and continuous reduction of rotational speed of generator rotor. However, with the DVR in operation, the turbine rotor speed is similar to the no fault speed as shown in Fig.38.

A DC-link capacitor provides temporary injection of the active power when the DC-link voltage decreases and vice versa. Fig. 39 and Fig. 40 demonstrate the influence of the sag voltage fault on the DC link voltage V_{dc} at the PV and WTG inverters.

In Fig. 39, the V_{dc} of the WTG inverter has drastically increased from its steady-state value of 1000 V at the beginning of the sag voltage fault to 5500 V at the end of the fault

and continued to increase after the fault is cleared to reach 6500 V at the end of the simulation.

Also Fig. 40 shows the dynamic behavior of the V_{dc} link voltage at the PV inverter during fault disturbance. It can be clearly seen that the V_{dc} has increased during the fault to 1250 V and then decreased until it reached 680 V which is below its reference voltage 714 V after the fault was cleared.

With the DVR contribution the V_{dc} link at PV and WTG inverters are identical to the no-fault case as shown in Fig. 39 and Fig.40.

VI. CONCLUSIONS

The simulation study was carried out using MATLAB to demonstrate the effectiveness of the proposed DVR control system to improve the power quality and LVRT capability of the hybrid PV-WT power system. The system has been tested under different fault condition scenarios. The results have shown that the DVR connected to the PV-Wind hybrid system at the medium voltage grid is very effective and is able to mitigate voltage outages and short circuit failure with improved voltage regulation capabilities and flexibility in the correction of the power factor.

The results of the simulation also prove that the system designed is secure since the required voltage ranges are respected correctly and the DG generators operate reliably.

The main advantage of the proposed design is the rapid recovery of voltage; the power oscillations overshoot reduction, control of rotor speed and preventing the system from having a DC link overvoltage and thus increasing the stability of the power system in accordance with LVRT requirements.

REFERENCES

[1] J. Hossain and H. R. Pota, *Robust Control for Grid Voltage Stability High Penetration of Renewable Energy*,1st ed. Singapore: Springer, 2014, pp. 1–11.

[2] S. Talari, M. Shafie-Khah, G. J. Osório, J. Aghaei, and J. P. S. Catalão, "Stochastic modelling of renewable energy sources from operators' point-of-view: A survey," *Renew. Sustain. Energy Rev.*, vol. 81, no. P2, pp. 1953–1965, Jan. 2018.

[3] R. Teodorescu, M. Liserre, and P. Rodríguez, *Grid Converters for Photovoltaic and Wind Power Systems*, 1st ed. Hoboken, NJ, USA: Wiley, 2011.

[4] G. R. Rey and L. M. Muneta, *Electrical Generation and Distribution Systems and Power Quality Disturbances*, 1st ed. Rijeka, Croatia: InTech, 2011.

[5] R. Li, H. Geng, and G. Yang, "Fault ride-through of renewable energy conversion systems during voltage recovery," *J. Mod. Power Syst. Clean Energy*, vol. 4, no. 1, pp, 28–39, 2016.

[6] S. Kirmani, M. Jamil, and I. Akhtar, "Economic feasibility of hybrid energy generation with reduced carbon emission," *IET Renew. Power Gener.*, vol. 12, no. 8, pp. 934–942, Nov. 2018.

[7] S. M. Muyeen, "A combined approach of using an SDBR and a STATCOM to enhance the stability of a wind farm," *IEEE Syst. J.*, vol. 9, no. 3, pp. 922–932, Sep. 2015.

[8] S. Ghosh and S. Kamalasadan, "An energy function-based optimal control strategy for output stabilization of integrated DFIG-flywheel energy storage system," *IEEE Trans. Smart Grid*, vol. 8, no. 4, pp. 1922–1931, Jul. 2017.

[9] G. Rashid and M. H. Ali, "Nonlinear control-based modified BFCL for LVRT capacity enhancement of DFIG-based wind farm," *IEEE Trans. Energy Convers.*, vol. 32, no. 1, pp. 284–295, Mar. 2017.

[10] M. K. Döşoğlu and A. B. Arsoy, "Transient modeling and analysis of a DFIG based wind farm with supercapacitor energy storage," *Int. J. Elect. Power Energy Syst.*, vol. 78, pp. 414–421, Jun. 2016.

[11] M. K. Döşoğlu, "Nonlinear dynamic modeling for fault ride-through capability of DFIG-based wind farm," *Nonlinear Dyn.*, vol. 89, no. 4, pp. 2683–2694, Sep. 2017.

[12] M. K. Döşoğlu, A. B. Arsoy, and U. Güvenç, "Application of STATCOM-supercapacitor for low-voltage ride-through capability in DFIG-based wind farm," *Neural Comput. Appl.*, vol. 28, no. 9, pp. 2665–2674, Sep. 2017.

[13] M. K. Döşoğlu, "Enhancement of SDRU and RCC for low voltage ride through capability in DFIG based wind farm," *Elect. Eng.*, vol. 99, no. 2, pp. 673–683, Jun. 2017.

[14] D. D.-C. Lu, *An Update on Power Quality*, 1st ed. Rijeka, Croatia: InTech, 2013.

[15] T. F. Orchi, M. J. Hossain, H. R. Pota, and M. S. Rahman, "Voltage stability and power quality issues of wind farm with series compensation," in *Proc. IEEE Elect. Power Energy Conf.*, Halifax, NS, Canada, Aug. 2013, pp. 1–6.

[16] K. Rajesh, A. Kulkarni, and T. Ananthapadmanabha, "Modeling and simulation of solar PV and DFIG based wind hybrid system," *Procedia Technol.*, vol. 21, pp. 667–675, Aug. 2015.

[17] O. Noureldeen and A. M. A. Ibrahim, "Modeling, implementation and performance analysis of a grid-connected photovoltaic/wind hybrid power system," in *Proc. Int. Conf. Innov. Trends Comput. Eng. (ITCE)*, Aswan, Egypt, Feb. 2018, pp. 296–304.

[18] H. Laabidi and A. Mami, "Grid connected wind-photovoltaic hybrid system," in *Proc. 5th Int. Youth Conf. Energy (IYCE)*, May 2015, pp. 1–8.

[19] Y. Zhu, J. Yao, and D. Wu, "Comparative study of two stages and single stage topologies for grid-tie photovoltaic generation by PSCAD/EMTDC," in *Proc. Int. Conf. Adv. Power Syst. Automat. Protection*, Beijing, China, Oct. 2011, pp. 1304–1309.

[20] M. Shayestegan, "Overview of grid-connected two-stage transformerless inverter design," *J. Mod. Power Syst. Clean Energy*, vol. 6, no. 4, pp. 642–655, 2018.

[21] N. G. F. Petrone, G. Spagnuolo, and M. Vitelli, *Power Electronics and Control Techniques for Maximum Energy Harvesting in Photovoltaic Systems*, 1st ed. Boca Raton, FL, USA: CRC Press, 2013.

[22] D. Verma, S. Nema, A. M. Shandilya, and S. K. Dash, "Maximum power point tracking (MPPT) techniques: Recapitulation in solar photovoltaic systems," *Renew. Sustain. Energy Rev.*, vol, 54, pp. 1018–1034, Feb. 2016.

[23] H. Abu-Rub, M. Malinowski, and K. Al-Haddad, *Power Electronics for Renewable Energy Systems, Transportation and Industrial Applications*, 1st ed. Hoboken, NJ, USA: Wiley, 2014.

[24] B. L. Dokić and B. Blanuša, *Power Electronics Converters and Regulators*, 3rd ed. Cham, Switzerland: Springer, 2015.

[25] N. Mohan, *Power Electronics*, 1st ed. Hoboken, NJ, USA: Wiley, 2012.

[26] N. Mohan, T. M. Undeland, and W. P. Robbins, *Power Electronics: Converters, Applications, and Design*, 3rd ed. Hoboken, NJ, USA: Wiley, 2003.

[27] S. Heier, *Grid Integration of Wind Energy: Onshore and Offshore Conversion Systems*, 1st ed. Hoboken, NJ, USA: Wiley, 2014.

[28] M. H. Ali, *Wind Energy Systems: Solutions for Power Quality and Stabilization*, 1st ed. Boca Raton, FL, USA: CRC Press, 2012.

[29] M. Mansour, M. N. Mansouri, and M. F. Mimouni, "Comparative study of fixed speed and variable speed wind generator with pitch angle control," in *Proc. Int. Conf. Commun., Comput. Control Appl. (CCCA)*, Mar. 2011, pp. 1–7.

[30] I. A. Gowaid, A. S. Abdel-Khalik, A. M. Massoud, and S. Ahmed, "Ride-through capability of grid-connected brushless cascade DFIG wind turbines in faulty grid conditions—A comparative study," *IEEE Trans. Sustain. Energy*, vol. 4, no. 4, pp. 1002–1015, Oct. 2013.

[31] O. Abdel-Baqi and A. Nasiri, "Series voltage compensation for DFIG wind turbine low-voltage ride-through solution," *IEEE Trans. Energy Convers.*, vol. 26, no. 1, pp. 272–280, Mar. 2011.

[32] R. A. J. Amalorpavaraj, P. Kaliannan, S. Padmanaban, U. Subramaniam, and V. K. Ramachandaramurthy, "Improved fault ride through capability in DFIG based wind turbines using dynamic voltage restorer with combined feed-forward and feed-back control," *IEEE Access*, vol. 5, pp. 20494–20503, 2017.

[33] N. G. Hingorani and L. Gyugyi, *Understanding FACTS: Concepts and Technology of Flexible AC Transmission Systems*, 1st ed. Piscataway, NJ, USA: IEEE Press, 2000.

[34] N. H. Woodley, L. Morgan, and A. Sundaram, "Experience with an inverter-based dynamic voltage restorer," *IEEE Trans. Power Del.*, vol. 14, no. 3, pp. 1181–1186, Jul. 1999.

[35] E. Acha, V. G. Agelidis, O. Anaya-Lara, and T. J. E. Miller, *Power Electronic Control in Electrical Systems*, 1st ed. Newnes, U.K.: Newnes Publisher, 2002.

[36] A. I. Al-Odienat and A. A. Al-Lawama, "The advantages of PID fuzzy controllers over the conventional types," *Amer. J. Appl. Sci.*, vol. 5, no. 6, pp. 653–658, 2008.
[37] P. Margo, M. P. Heri, M. Ashari, and T. Hiyama, "Balanced voltage sag correction using dynamic voltage restorer based fuzzy polar controller," in *Proc. 2nd Int. Conf. Innov. Comput., Inf. Control (ICICIC)*, Kumamoto, Japan, Jan. 2007, p. 93.
[38] S. P. Singh, A. H. Bhat, and A. Kumar, "Fuzzy logic based dynamic voltage restorer for addressing various power quality problems," in *Proc. IEEE 7th Power India Int. Conf. (PIICON)*, Bikaner, India, Nov. 2016, pp. 1–5.
[39] R. H. Salimin and M. S. A. Rahim, "Simulation analysis of DVR performance for Voltage sag mitigation," in *Proc. 5th Int. Power Eng. Optim. Conf.*, Selangor, Malaysia, Jun. 2011, pp. 261–266.
[40] R. Rajeswari, N. Karpagam, and S. Dhanalakshmi, "Analysis of dq0 based fuzzy logic controller in DVR for voltage sag and harmonic mitigation," in *Proc. Int. Conf. Green Comput. Commun. Elect. Eng. (ICGCCEE)*, Mar. 2014, pp. 1–6.
[41] H. P. Tiwari and S. K. Gupta, "DC energy storage schemes for DVR voltage sag mitigation system," *Int. J. Comput. Theory Eng.*, vol. 2, no. 3, p. 313, Jun. 2010.
[42] J. Hossain and A. Mahmud, *Large Scale Renewable Power Generation*, 1st ed. Singapore: Springer, 2014.
[43] F. Shahnia, S. Rajakaruna, and A. Ghosh, *Static Compensators (STATCOMs) in Power Systems*, 1st ed. Singapore: Springer, 2015.
[44] F. Kalverkamp, B. Schowe-von der Brelie, T.-D. Nguyen, T. Mertens, and M. Meuser, "Comparative analysis of European grid codes and compliance standards for distributed power generation plants with respect to future requirements of ENTSO-E and CENELEC," in *Proc. Int. ETG Congr., Die Energiewende-Blueprints New Energy Age*, Nov. 2015, pp. 1–6.
[45] A. Q. Al-Shetwi, M. Z. Sujod, and N. L. Ramli, "A review of the fault ride through requirements in different grid codes concerning penetration of PV system to the electric power network," *ARPN J. Eng. Appl. Sci.*, vol. 10, no. 21, pp. 9906–9912, 2015.

ABDELKRIM BENALI received the M.A. degree in electrotechnics from the Polytechnic National School of Oran, Algeria. He is currently a Professor with the Department of Electrical Engineering, NOUR Bachir university Center, El Bayadh, Algeria. He is a member of the SCAMRE Laboratory, ENP. His research activities include FACTS devices, renewable energy and distributed energy resources modeling and conception, and renewable energy grid integration.

MOUNIR KHIAT received the Ph.D. degree in electrotechnics from the University of USTO, Oran. He is currently a Professor with the Department of Electrical Engineering, Polytechnic National School of Oran, Algeria. He is a member of the SCAMRE Laboratory, ENPO. His research activities include the control of large electric power systems, multi machine, multi converter systems, FACTS devices, HVDC systems, renewable energy and distributed energy resources, modeling and conception, real-time simulation of power systems, smart grids, neural process control, and real-time simulation of power systems.

TAYEB ALLAOUI received the bachelor's (Engineering) degree in electrical engineering from the Ibn Khaldoun University of Tiaret in 1996 and the master's degree from the University of Science and Technology of Oran in 2002. He is a member of the Energetic Engineering and Computer Engineering Laboratory, Ibn Khaldoun University. His research interests include intelligent control of power systems and FACTS, active filter, and renewable energies.

MOULOUD DENAÏ graduated from the University of Science and Technology of Algiers and the École Nationale Polythechnique of Algiers, Algeria, in electrical engineering, and received the Ph.D. degree in control engineering from The University of Sheffield, U.K. He was with the University of Science and Technology of Oran, Algeria, until 2004. From 2004 to 2010, he was with The University of Sheffield. From 2010 to 2014, he was with the University of Teesside, U.K. Since 2014, he has been with the University of Hertfordshire, U.K. His main fields of expertise are in modeling, optimization, and control of engineering and life science (biological and biomedical) systems. His current research interests in energy include intelligent control design and computational intelligence applications to efficiency optimization in renewable energy systems with particular focus in the management of smart homes and dynamic scheduling, optimization and control of future smart grids, condition monitoring and asset management in electric power networks; energy storage systems integration into the grid; smart meter data analytics using machine learning techniques for efficient energy management; electric vehicles integration into the distribution grid; and V2G/G2V management.